Journal of Alloys and Compounds 526 (2012) 45–52

Contents lists available at SciVerse ScienceDirect

Journal of Alloys and Compounds

journal homepage: www.elsevier.com/locate/jallcom

Microstructure, mechanical and functional properties of NiTi-based shape memory ribbons

K. Mehrabi[a,*], M. Bruncko[a,b], A.C. Kneissl[a]

[a] Department of Physical Metallurgy and Materials Testing, University of Leoben, Austria
[b] Faculty of Mechanical Engineering, University of Maribor, Slovenia

ARTICLE INFO

Article history:
Received 26 November 2011
Received in revised form 12 February 2012
Accepted 13 February 2012
Available online xxx

Keywords:
Shape memory alloys
NiTi-based alloys
Two-way effect
Melt-spinning
Thermomechanical training
Microstructure

ABSTRACT

The present work has been aimed to study the microstructures, functional properties and the influence of different thermomechanical training methods on the two-way shape memory effect in NiTi-based melt-spun ribbons. In order to get small-dimensioned shape memory alloys (SMAs) with good functional and mechanical properties, a rapid solidification technique was employed. Their fracture and elasticity characteristics have been determined, as well as shape memory properties by thermomechanical cycling. The ribbons were trained under tensile and bending deformation by thermal cycling through the phase transformation temperature range.

The results displayed that all different training methods were effective in developing a two-way shape memory effect (TWSME). The influence of copper (5–25 at.% Cu) and tungsten (2 at.% W) on the microstructure, and the functional and mechanical behavior of NiTi thin ribbons was also investigated. All samples show a shape memory effect immediately after processing without further heat treatment. The melt-spun ribbons were trained under constant strain (bending and tensile deformation) by thermal cycling through the phase transformation temperature range. The addition of copper was effective to narrow the transformation hysteresis. The W addition has improved the TWSME stability of the NiTi alloys and mechanical properties. Results about microstructures, functional and mechanical properties will be presented.

© 2012 Elsevier B.V. All rights reserved.

1. Introduction

In recent years shape memory alloys (SMAs) have been recognized as effective and promising means for application in various branches of engineering, e.g. space technology, medicine, robotics and actuator technology. For the usage of SMAs in thermosensitive devices, it is very important to increase the speed of response and the sensitivity of shape memory elements, as well as to widen essentially the application fields of thermosensors through their miniaturization. Hence, there is a trend to very small-dimensioned shape memory elements, which could be used as microactuators. One of the perspective materials for this purpose is SMA rapid solidificated ribbon.

There are several advantages of rapid solidification over the slower conventional solidification techniques. These are an ability to form metastable phases, enlarging the third element addition range and increasing the solubility above the equilibrium solubility, decreasing the segregation of additions, and refining the microstructure, which can favor the ductility and shape memory characteristics.

In these applications the NiTi components often experience repeated transformation cycles, either under external load or free of constraint. One critical concern in the development of such devices is the stability of the shape memory properties. Obviously, unstable transformation cycles with associated difficulties with respect to accurate predictions of materials behavior and device design are not desirable for actuator applications.

From the several modes of shape memory effect, the two-way shape memory effect (TWSME) is the most suitable to apply in actuators since no resetting force has to be considered in design. However, it is not inherent to SMAs, but can be exhibited after specific repetitive thermomechanical treatments known as training procedures through which SMAs memorize the low temperature shape. To date, more than 20 different training procedures have been investigated and published in efforts to develop a TWSME of both high magnitude and stability, which have the common feature that external applied stress should be used, such as tension, compression, torsion or bending. There are some training methods without applied load, which induce internal stress by quenching, ion irradiation or external magnetic fields [1]. It is generally

* Corresponding author at: Department of Physical Metallurgy and Materials Testing, University of Leoben, 8700 Leoben, Styria, Austria. Tel.: +43 3842 4024250; fax: +43 3842 4024202.
E-mail address: kambiz.mehrabi@unileoben.ac.at (K. Mehrabi).

0925-8388/$ – see front matter © 2012 Elsevier B.V. All rights reserved.
doi:10.1016/j.jallcom.2012.02.097

perceived that the development of TWSME originates from the preferential nucleation and growth of martensite variants that are essentially guided by the internal stress field [2]. During the training process, the resulting stress field assists the formation and growth of preferentially oriented martensite variants when the martensitic transformation proceeds in a specimen on cooling [3].

The most popular ones are thermal cycling under constant strain or stress. Constant strain training using tensile and bending deformation is advantageous for shape memory elements with more complicated shapes, while constant stress training is limited to linear shape changes. Tensile training was carried out through the repetition of several thermal cycles under a uniaxial tensile load to specified strain. Also bending training method was applied to NiTi-based ribbons in comparison with the tensile training and evaluation of the long-term TWSME stability, which consists of several thermal cycles under constant bending strain followed by load-free thermal cycling. The TWSME was executed several thousand times and the changes in the deformation behavior and the stability of the effect were continuously observed.

The near equiatomic NiTi alloys are by far the most widely used shape memory materials, but the relatively large transformation hysteresis of about 30 °C can be inconvenient for some applications. Substituting Cu for Ni in binary Ni–Ti makes smaller transformation hysteresis, lower flow stress level in the martensite state. Because of the aforementioned advantages, ribbons of NiTiCu SMAs would be a good candidate for applications that require short response time at thermal cycle, such as actuators and sensors. Also the Cu additions to NiTi cause a reduction in the strong sensitivity of the transformation temperatures to small variations in the Ni content and they suppress electric resistivity, thus allowing for better actuator control [4]. Most important, they improve geometrical and thermal actuator stability, because of a better crystallographic compatibility between the parent and the product phase. There is a good correlation between the width of the thermal hysteresis and the intensity of irrecoverable deformation associated with thermomechanical cycling.

In NiTiCu alloys with more than 10 at.% Cu the B2 → B19 transformation is observed. The B2 (cubic) → B19(orthorhombic) martensitic transformation is known to be very suitable for actuators because of its large transformation elongation and small hysteresis. This transformation has been also observed in NiTiPd and NiTiAu alloys, but from these additions Cu is the most attractive from an economic point of view. Transformation hysteresis accompanied by the B2 → B19 transformation in NiTiCu alloys decreases with increasing Cu content due to a decrease in lattice deformation. Therefore, NiTiCu alloys with high Cu content are desirable for actuators that operate sensitively according to a temperature change.

However, NiTiCu alloys with Cu content higher than 10 at.% are brittle due to the TiCu phase formed near the grain boundaries, and therefore cannot be deformed into a wire or plate by both hot and cold working, which is necessary for fabricating actuators. In order to overcome the brittleness of the alloys, many metallurgical processing technologies have been examined, including powder metallurgy and rapid solidification [5]. The melt-spinning process could be one of the best alternatives for fabricating NiTiCu alloys with high Cu content because it enables ribbons to be obtained directly from the molten metal, and the high solidification rate suppresses the formation of TiCu particles.

It is reported that the shape recovery of NiTi alloys can be increased by different strengthening processes [6]. In other words, if the matrix is strengthened, the slip of dislocations is more difficult than the movement of twin boundaries during the application of external stress. From there, the permanent plastic strain is reduced and the shape recovery can be improved. The matrix of NiTi alloys is strengthened by the addition of tungsten, and because of the low solubility of W in NiTi, as little as 2 at.% W (corresponds to 6.6 wt.% W) is enough to obtain W-rich precipitates in the NiTi matrix [7]. Partial substitution of Ni by W has only small influences on the transformation temperatures and transformation hysteresis in contrast to other elements such as Cu, Hf, Nb, etc.

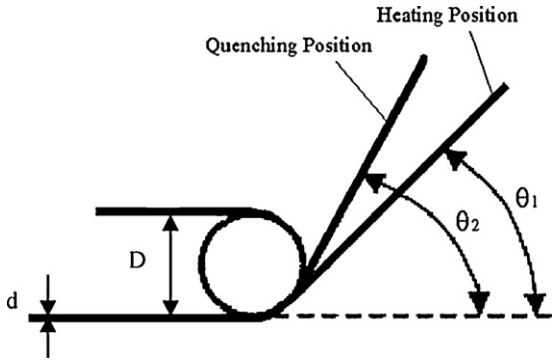

Fig. 1. Schematic illustration for bending examination of TWSME.

In the present study, the microstructure, mechanical properties and shape memory characteristics of three different alloy systems (NiTi, NiTiCu and NiTiW), fabricated by melt-spinning were investigated.

2. Experimental procedures

The NiTi alloy ingots were prepared by vacuum arc-melting on a water-cooled copper hearth in a reduced Ar atmosphere. To ensure homogeneity, arc-melting was repeated three times for each alloy. Three different alloy systems were used: (1) binary NiTi, which represents a standard SMA; (2) ternary NiTiCu (with 5 and 25 at.% Cu); (3) a dual phase alloy consisting of a NiTi matrix containing precipitates of tungsten to investigate the influence of second phase particles.

The melt-spun ribbons were produced under a 200 mbar He atmosphere using quartz-glass crucibles with a nozzle diameter of 0.9 mm, coated internally with Y_2O_3. By applying an Ar overpressure of ~90 mbar within the crucible, the melt was ejected onto the surface of a polished Cu wheel (200 mm diameter) having a circumferential wheel speed of 5–50 m/s. The distance between the nozzle and the wheel surface was from 0.6 to 2 mm. Table 1 gives the chemical compositions (at.%) of the ribbons and melt-spinning parameters.

For bending training and stability of the TWSME with this method, the bending deformation strain (ε_d) of the outer surface of the specimen was calculated using the equation $\varepsilon_d = d/(D+d)$, where d is the ribbon thickness and D is the diameter of the constrained circle. The one-way shape recovery strain (ε_{1w}), two-way shape memory strain (ε_{2w}) and plastic deformation (η_p) were measured by the values of $\varepsilon_{1w} = [(\theta_0 - \theta_1)/\theta_0] \times \varepsilon_d$, $\varepsilon_{2w} = [(\theta_2 - \theta_1)/\theta_0] \times \varepsilon_d$ and $\eta_p = \theta_1/\theta_0$, respectively, where the angle $\theta_0 = 180°$ and the deformation angles θ_1 and θ_2 are indicated in Fig. 1.

The value of spontaneous shape change during heating and cooling was recorded by photographs. The thermal cycling is through the phase transformation temperature range (from room temperature to 170 °C in the case of NiTi(W) and NiTi5Cu samples and from room temperature to 120 °C in the case of NiTi25Cu samples).

Specimens for SEM and optical metallographic investigation were cut from the longitudinal cross sections of melt-spun ribbons. They were ground on SiC paper to a final mesh size of 4000 and polished with 3 μm, 1 μm and OP-S suspensions. The samples were etched in a solution containing 100 ml H_2O, 25 ml C_2H_6O, 2 g NH_4HF_2 (modification of Weck's reagent) with etching

Table 1
The chemical compositions of the ribbons and melt-spinning parameters.

No.	Ribbons	Ni	Ti	W	Cu	Crucible/wheel distance mm	Wheel speed m/s	Melting temperature °C
1	NiTi	49.7	50.3	–	–	2	15	1450–1500
2	NiTi2W	47.7	50.3	2	–	2	15	1550–1600
3	NiTi5Cu	44.7	50.3	–	5	2	20	1350–1400
4	NiTi25Cu	24.7	50.3	–	25	0.6	25	1300–1350

times between 2 and 15 s and then studied by optical microscopy using interference contrast. For TEM studies thin discs, (3 mm in diameter), were mechanically ground to a thickness of 60 μm and polished in an electrolyte consisting of 20% sulphuric acid and 80% methanol at 0–5 °C by a twin jet electro-polisher [8]. Ion-milling was then performed on the samples for 30 min. The energy of the Ar+ ions was 3.6 keV, the angle to the surface of the specimen was ±4°, and the specimen was kept at a rotation rate of 3 rpm during ion-milling. Conventional TEM studies were performed on a Philips CM12 at an acceleration voltage of 120 kV. Additionally, the chemical composition of the samples was examined with a TEM, equipped with an EDX analyzer.

Tensile specimens with gauge size of 20–30 mm in length and 2–4 mm in width were cut from the melt-spun ribbons and tensile tests have performed using a miniature tensile device built by Kammrath & Weiss GmbH. The samples were loaded at a temperature at least below A_s to detwin the martensite. After unloading, the sample is heated to recover austenite and the original shape.

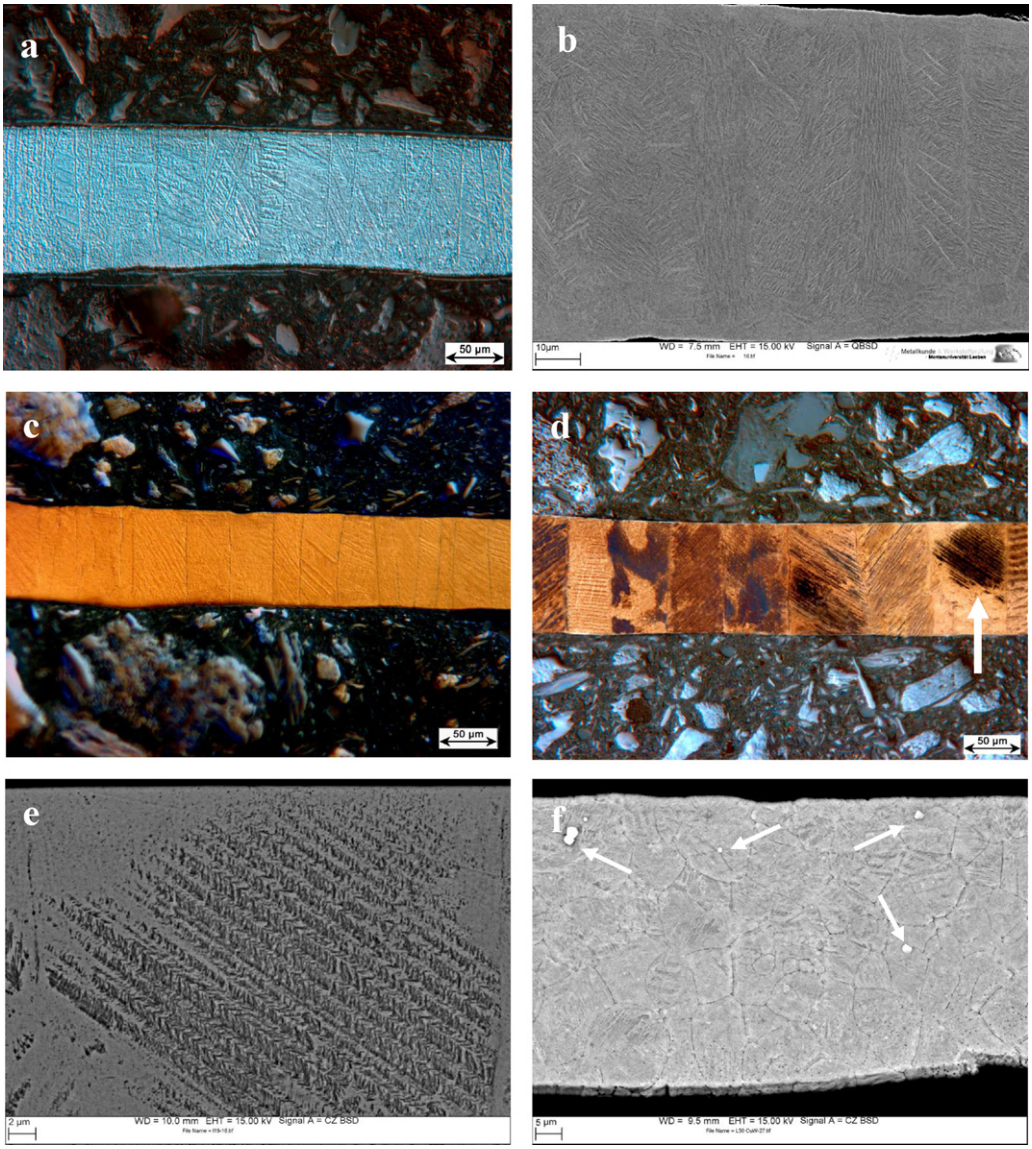

Fig. 2. Microstructures of ribbons: (a) optical microstructure of a NiTi ribbon; (b) SEM micrograph of NiTi; (c) NiTi5Cu ribbon; (d) NiTi25Cu ribbon; (e) SEM image of the region of (d) indicated by an arrow showing twin boundaries; (f) SEM micrograph of NiTiW with multi-layer structure and dissolved W-particles (arrows).

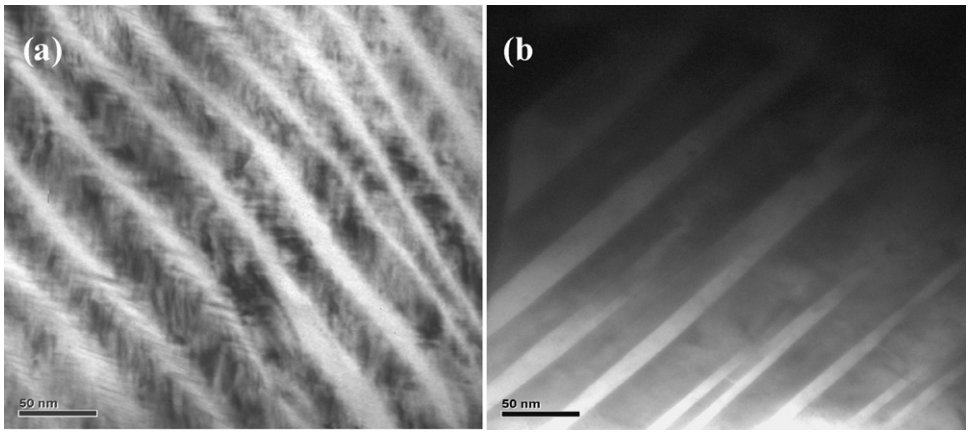

Fig. 3. TEM images of ribbons: (a) B19′ martensite of NiTi and (b) B19 martensite of NiTiCu.

Tensile tests were completed at a constant temperature between 25 °C and 200 °C, to determine the stress–strain properties of the ribbons.

3. Results and discussion

3.1. Etchants and microstructures

It was observed that the increase in the wheel speed from 5 to 45 m/s results in a decrease in the ribbon thickness from ~100 to ~20 μm. As the increase in the wheel speed leads to a reduced ribbon thickness, the cooling rate increases and therefore the martensitic substructure gets finer. All of the samples exhibited a fully crystallized microstructure and shape memory effects immediately after processing. Only in NiTi25Cu at a wheel speed of 45 m/s amorphous structures were obtained.

Fig. 2 shows the micrographs of NiTi, NiTi5Cu, NiTi25Cu and NiTiW ribbons produced by melt-spinning at medium wheel speeds (Table 1). In NiTi25Cu (Fig. 2d and e), no second phase, such as TiCu, was observed in our samples, even though the Cu content of the alloy exceeds the Cu solubility limit by far, while it was observed near grain boundaries in conventional casting [5]. In addition, some regions of NiTi25Cu ribbons clearly consist of twins such as the marked region in Fig. 2d. The twin-like substructure of the martensite can be seen partially already with the SEM using back scattered electrons (Fig. 2e) in the NiTi25Cu sample. Additionally, it was shown in NiTiW ribbons (Fig. 2f) that the microstructures are not always single-layer columnar structure, which is characteristic for melt-spun ribbons, but sometimes multi-layer structure with random grain orientation.

TEM was employed to investigate martensitic structures of ribbons, which are too fine to be sufficiently resolved with SEM. Fig. 3a and b displays monoclinic B19′ structure of NiTi ribbon and orthorhombic B19 structure of NiTiCu ribbon, respectively. In NiTi ribbon, the twin-like substructure of the martensite is nano-sized and could be revealed only using TEM. Therefore, the martensite in NiTi ribbons is much finer than the martensite in NiTiCu.

3.2. Stress–strain curves

In Fig. 4, four different NiTi-based ribbons were tested to failure at 25 °C. The stress–strain behaviors of the ribbons are similar and follow typical tensile deformation characteristics in NiTi materials. It can be clearly seen that all the ribbons show a martensitic plateau without any subsequent heat treatment. After the stress plateau the curves show a rapid increase of the stress mainly due to the deformation of the detwinned structure. Practically, after the stress plateau, the deformation behavior of the alloy becomes similar to that of traditional structural materials; most of the specific applications of the NiTi-based alloys lie in the stress plateau. As shown in the figure, NiTiW and NiTiCu ribbons reveal, respectively, a higher and lower tensile strength than NiTi ribbons in the plateau regions.

The pseudoplastic deformation reaches about 3–4% strain before plastic deformation occurs, however, for a polycrystalline matrix an exact definition of the different zones is difficult due to the coexistence of the several mechanisms associated with the deformation process. The NiTi-based ribbons fracture at a strain between 6% and 7%.

The different alloys have revealed differences in strength, critical stresses and yielding points. In order to understand the difference in mechanical properties of various NiTi-based ribbons, several factors need to be considered, such as grain size, martensite microstructure, crystal structure and precipitates. For example, the martensite in NiTi, NiTiW and NiTi5Cu has a monoclinic unit cell while that of the NiTi25Cu has an orthorhombic unit cell.

Fig. 5 shows the mechanical properties of an amorphous NiTi25Cu melt-spun ribbon. Amorphous ribbons without any crystal phases were produced only in NiTi25Cu alloy under high cooling rates at a wheel speed of 45 m/s. The amorphous ribbons exhibit higher fracture strength and Young's modulus than the crystallized ribbons. This is caused by the absence of mobile defects and this elastic-type behavior is well known for amorphous alloys [9,10]. Several thermal cycles (up to 220 °C) were performed at 2% strain

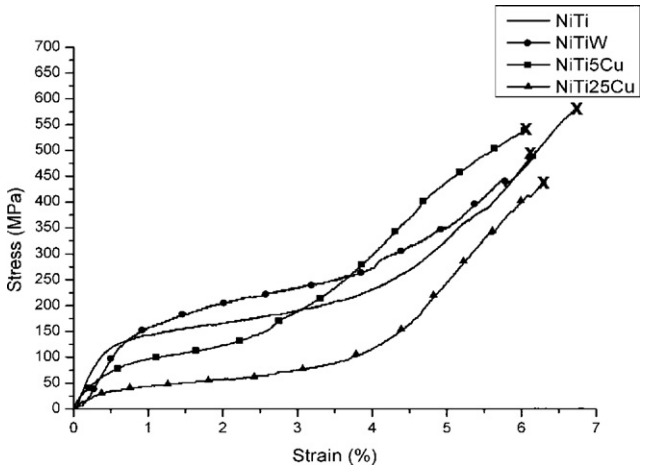

Fig. 4. Stress–strain curves of the different alloys. The symbol (x) represents the fracture point.

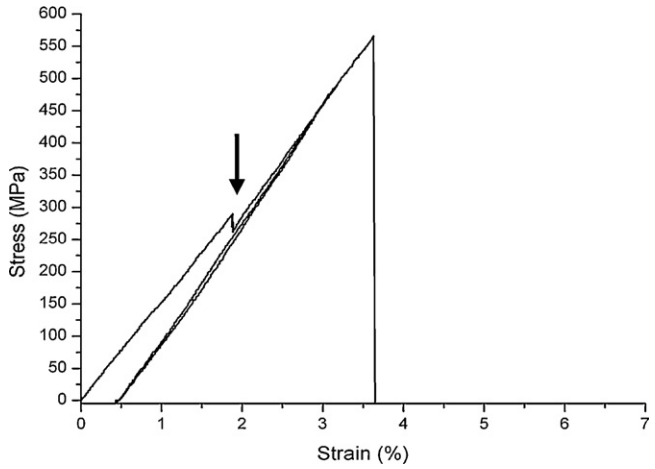

Fig. 5. Tensile test result for amorphous NiTi25Cu ribbons at wheel speed of 45 m/s.

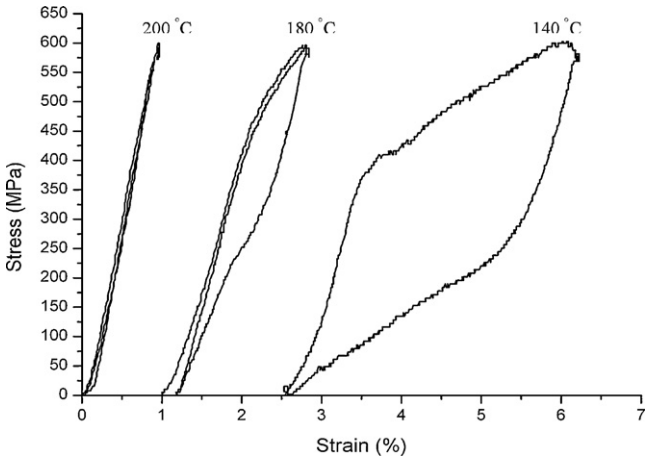

Fig. 7. Stress–strain curves of NiTi ribbons at different austenitic temperatures.

(arrow) to find out if the microstructure changes (i.e. crystallizes), but an unloading-reloading test up to 3% strain showed that evidently there is no change.

A stress–strain curve of NiTi at 140 °C which is above A_f temperature can be seen in Fig. 6a. Also Fig. 6b shows stress–strain curves of a NiTi25Cu ribbon tested first at 110 °C which is above A_f and then at room temperature. One unloading and reloading was carried out to see whether the ribbon is fully martensitic with pseudoplastic effect or not. It can be seen that the elastic modulus of austenite is higher than that of martensite. At low temperature, the SMA is in its soft martensitic phase; thus, it is easy to deform. But as the temperature increases above A_s, the structure becomes austenitic and stiffer and, therefore, more difficult to deform, requiring a greater stress to obtain the same strain values as in martensitic structure.

Fig. 7 demonstrates the stress versus strain behavior of the NiTi ribbons at different temperatures above A_f to find the M_d temperature, which is the maximum temperature to induce martensite by stress (pseudoelasticity). At temperatures greater than 160 °C and especially at 200 °C, ribbons do not exhibit pseudoelastic effect during unloading–reloading since the temperature of the ribbon is above M_d.

3.3. One-way shape memory effect

The melt-spun ribbons display the shape memory effect, which was easily observed by bending a ribbon and watching it return to its original shape upon heating. This SME also has been evaluated by room temperature tensile test.

Fig. 8 shows the stress–strain curves of three NiTi ribbons, which were loaded to stresses of 200, 250 and 450 MPa at room temperature, well below the A_s temperature of 72 °C. After unloading, 28%, 18% and 15% of the imparted strain was recovered elastically. The pseudoplastic deformation reaches about 4% strain before plastic deformation occurs. The curves at loading higher than a critical stress unload to a non-zero strain; however, these strains are recoverable on heating. The arrows indicate the recovery strains.

The total strain of the first ribbon is 2.4% with a recovery rate of 100%. The total strain of the second ribbon is much higher, which is 4.5%, with recovery strain of 4.1%, i.e. 91% recovery. The third ribbon was deformed to a total strain of 5.5% without fracture; however, the SME is lower with recovery strain of 3.7%, which is 67% recovery.

As shown in Fig. 9, two NiTi25Cu ribbons were loaded at room temperature to a strain of 3.4% and 6.2% at about 100 MPa and 250 MPa, respectively. After heating, the reverse martensitic transformation occurs, and the ribbon recovers its extension. The first ribbon was fully recovered and the second one recovered only partially (with recovery strain of 3.3%), as shown by arrow. The lower recovered strain obtained in this alloy is due to the formation of B19 martensite, which has a lower intrinsic transformation strain compared to the B19′ martensite.

Fig. 10 shows representative stress–strain curves for NiTiW and NiTi5Cu ribbons at room temperature. After heating, 4.2% and 4% strains were recovered, respectively, which are similar to NiTi ribbons. At certain strains the samples was deloaded and reloaded several times to determine if the material was fully pseudoplastic or not. The result reveals that there is no austenitic phase and pseudoelastic effect at all. In comparison to Fig. 10, Fig. 11 indicates some austenitic phase and pseudoelasticity in a NiTiW ribbon at

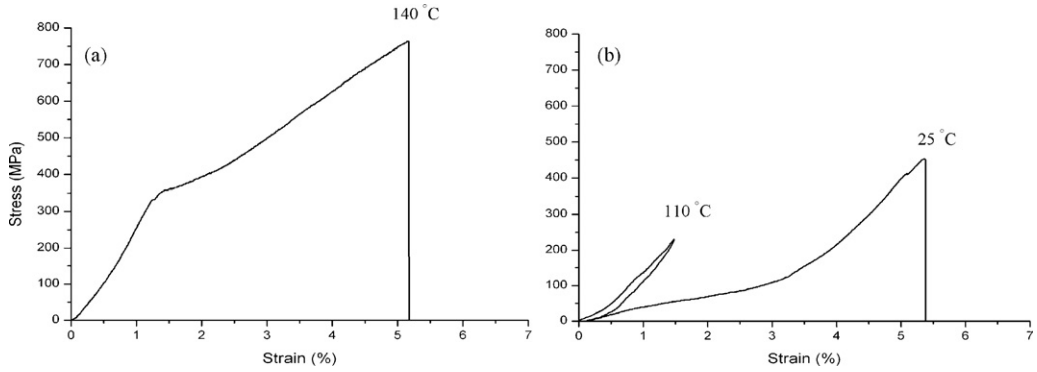

Fig. 6. Stress–strain curve of (a) NiTi ribbon at austenitic state and (b) NiTi25Cu ribbon tested at austenitic and martensitic states.

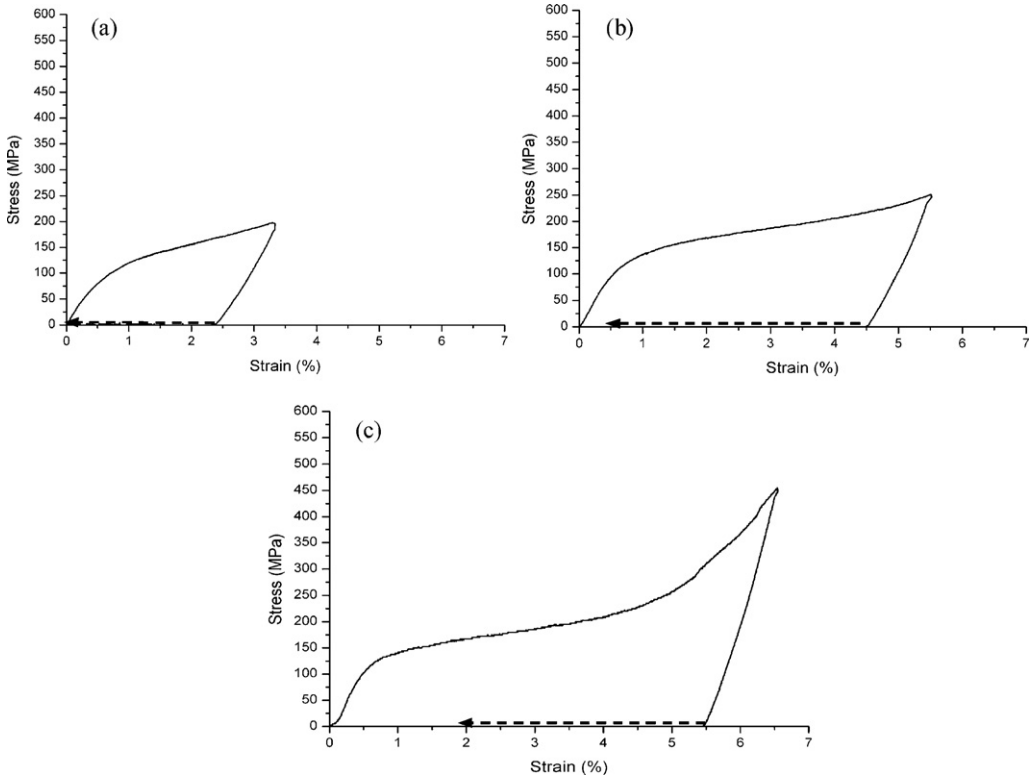

Fig. 8. Stress–strain curves of NiTi ribbons loading to maximum stresses of (a) 200 MPa, (b) 250 MPa and (c) 450 MPa at room temperature, indicating different recovery strains after heating. Dashed lines represent the recovered strain upon heating to 180 °C.

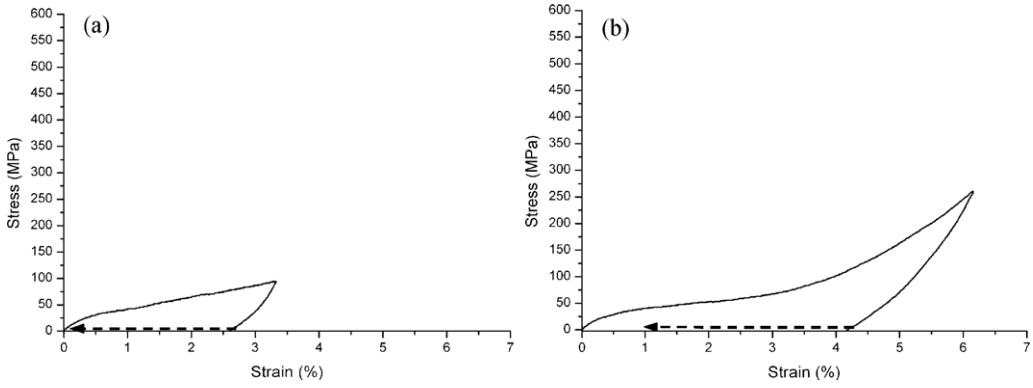

Fig. 9. Stress–strain curves of NiTi25Cu ribbons loading to maximum stresses of (a) 100 MPa and (b) 250 MPa at room temperature, indicating the one-way effect after heating.

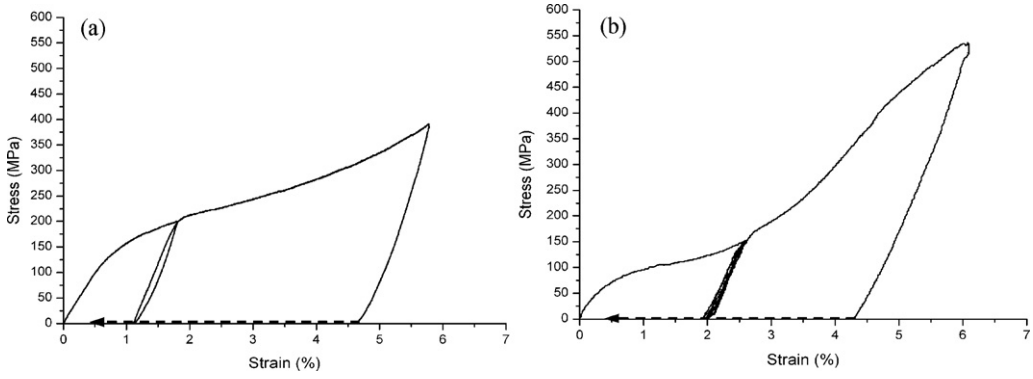

Fig. 10. Stress–strain curves of (a) NiTiW and (b) NiTi5Cu ribbons.

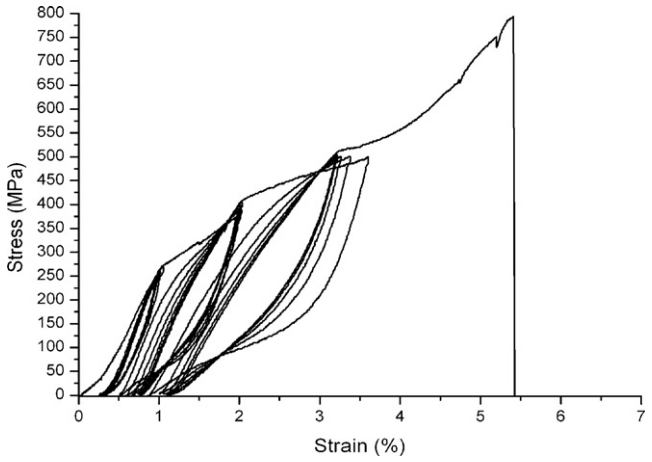

Fig. 11. Hysteresis cycles result for a NiTiW ribbon at 70 °C temperature.

70 °C (higher than A_s temperature). Close observation of this figure shows that the loading and unloading slopes are increased at each cycle because stress-induced martensite is stabilized and does not recover to austenite after unloading; this causes the decrease in the pseudoelasticity upon unloading.

3.4. Tensile training and TWSME

For the training experiments with tensile deformation, the ribbons were strained in the range of 3–6.5% in fully martensite state at room temperature. Fig. 12 shows the thermomechanical behavior of a NiTi ribbon at a constant strain of 3.5% and thermally cycled 5 times (segments 1 to 8) in comparison with NiTi25Cu ribbon, which have a much smaller transformation hysteresis than other NiTi-based alloys. The lower hysteresis obtained in the NiTi25Cu alloy is due to the formation of B19 (orthorhombic) martensite instead of B19′ (monoclinic) martensite, which has a lower intrinsic transformation strain [11]. It can be seen that NiTi25Cu ribbons exhibit better repeatability and stability during thermal cycles than NiTi ribbons, which show irreversible stresses.

After training, the specimens were unloaded and the shape change upon free thermal cycling – representing the induced intrinsic TWSME – was determined. Fig. 13 presents TWSME of NiTi ribbons and NiTi25Cu ribbons with various constant strains.

3.5. Bending training and stability of the TWSME

In bending training method, pieces of NiTi-based ribbons (~40 mm long and 2–4 mm wide) were bent to a small radius (about 0.9 mm) with a surface strain of 8% and cycled through the transformation range several times (3–15 times) in a constrained condition. The resulting two-way effect increases during the first few training cycles but afterwards decreases because the plastic deformation increases strongly. The opposite effect has been found during the free thermal cycles. This fact suggests that an appropriate density of slip defects is effective for the improvement of the TWSME while an excessive density of defects and plastic deformation reduce the TWSME.

Fig. 14 shows the stability of TWSME obtained by constrained training in some NiTi-based ribbons. In most cases, after enough constrained training and then several hundred free thermal cycles, the TWSME became larger with higher shape recovery and finally stabilized.

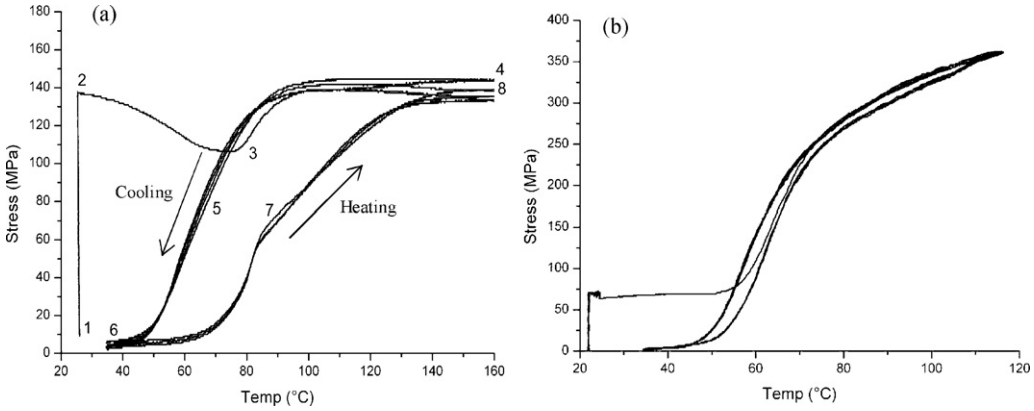

Fig. 12. Thermomechanical behavior at a constant strain of 3.5% after 5 thermal cycles (a) NiTi ribbon and (b) NiTi25Cu ribbon.

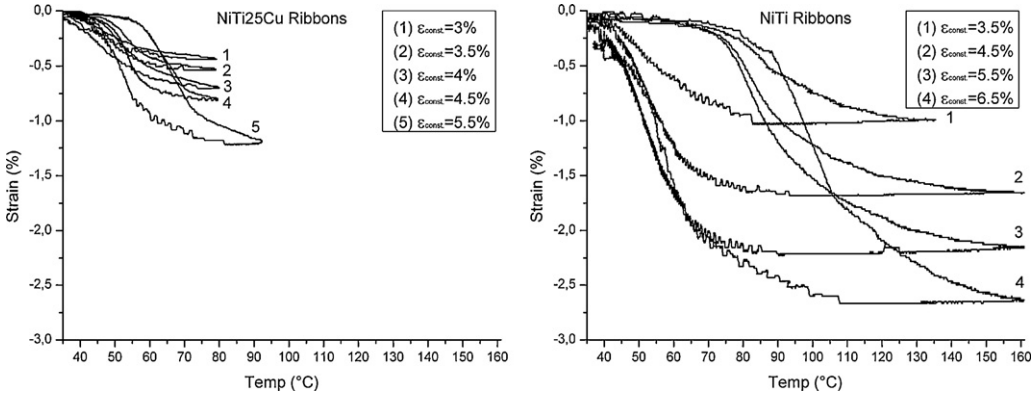

Fig. 13. TWSME exhibited in thermal cycles after training with various constant strains.

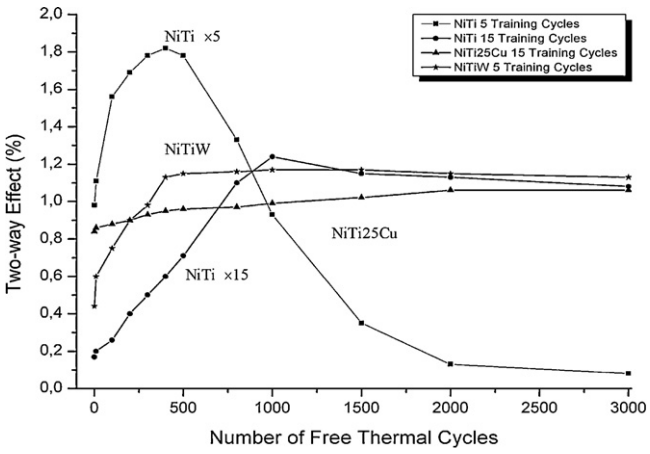

Fig. 14. Effect of free thermal cycles in different NiTi-based ribbons on TWSME.

As represented in the figure, the TWSME of NiTi ribbon trained with 5 constrained cycles was about 1%, after 400 free thermal cycles the size of TWSME increased steadily to reach a maximum of about 2%, but shows poor stability during the subsequent thermal cycling.

The decrease of TWSME in NiTi ribbons after a high number of thermal cycling may be related to partial relaxation of the stress field or rearrangement of dislocations formed by the training process and the redistribution of existing defects (dislocations). With a lowered density of dislocations, the internal stress field is not sufficient to ensure a favored variant to form.

However, when the training procedure is extended to 15 cycles, despite a smaller initial TWSME, the sample shows relatively high stability during 3000 thermal cycles. Similar to NiTi ribbon, the NiTi5Cu and NiTi25Cu ribbons demonstrated that 5 training cycles were not effective enough to stabilize TWSME and a good stability can be got only after 15 training cycles, however, the NiTi2W ribbon leads to a TWSME with proper stability already after 5 training cycles (ε_{2w} = 1.15%). This is due to higher strength of NiTi2W ribbon, which causes enough internal stress fields already after 5 training cycles.

Softer ribbons can be trained easily to higher effect size but the stability is weak. On the other hand, ribbons of higher strength exhibit smaller TWSME values but prove to be relatively stable against functional fatigue. The stability of about 1% TWSME in these ribbons seems very suitable for many applications.

4. Conclusions

- Melt-spun samples exhibited martensite structure and shape memory effects immediately after processing without subsequent heat treatment at room temperature, and they would be a good substitute for the conventionally cast alloys.
- The higher the wheel speed the lower is the thickness of the resulting ribbon and therefore the higher is the cooling rate. With increasing cooling rate the microstructure gets finer and finer and, therefore, metallographic preparation is not easy at all.
- Using a new etchant (modification of Weck's reagent) and interference contrast, it is possible to reveal the fine microstructures and grain boundaries. By SEM investigations of NITi25Cu the twin boundaries of the martensitic substructure could be shown. The martensite structure in binary NiTi, however, is much finer, and nano-sized twin boundaries could be revealed using TEM only.
- The one-way shape memory effect or recovery strain degrades with the increase of total tensile strain at room temperature.
- Two-way shape memory effects have been successfully introduced by different thermomechanical training methods in NiTi, NiTiCu and NiTiW alloys, which can be used for several applications, e.g. microsensors and microactuators.
- The addition of copper was effective to narrow the transformation hysteresis and the W addition has improved the stability of the TWSME and mechanical properties.
- The lower the strength of a ribbon the higher is the TWSME immediately after training but the stability is weak. On the other hand, ribbons of higher strength exhibit smaller TWSME values but prove to be relatively stable against functional fatigue.

References

[1] X.M. Zhang, J. Fernandez, J.M. Guilemany, Mater. Sci. Eng. A 438–440 (2006) 431–435.
[2] K. Wada, Y. Liu, Mater. Sci. Eng. A 481–482 (2008) 166–169.
[3] Ch.Y. Chang, D. Vokoun, Ch.T. Hu, Metall. Mater. Trans. A 32 (2001) 1629.
[4] Ch. Grossmann, J. Frenzel, V. Sampath, T. Depka, G. Eggeler, Metall. Mater. Trans. A 40 (2009) 2530–2544.
[5] S.W. Kang, Y.M. Lim, Y.H. Lee, H.J. Moon, Y.W. Kim, T.H. Nam, Scr. Mater. 62 (2010) 71–74.
[6] S.F. Hsieh, S.K. Wu, H.C. Lin, C.H. Yang, J. Alloys Compd. 387 (2005) 121–127.
[7] A.C. Kneissl, K. Mehrabi, M. Bruncko, B.J. McKay, D. Uhlenhaut, Int. J. Mater. Res. (Z. Metallkd.) 100 (2009) 1038–1045.
[8] L.J. Chiang, C.H. Li, Y.F. Hsu, W.H. Wang, J. Alloys Compd. 462 (2008) 47–51.
[9] A. Sezonenko, V. Kolomytsev, M. Babanly, A. Pasko, P. Ochin, R. Potier, P. Vermaut, J. Phys. IV 112 (2003) 889–892.
[10] A. Inoue, Mater. Sci. Eng. A 269 (1999) 171–183.
[11] R. Santamarta, E. Cesari, J. Pons, T. Goryczka, Metall. Mater. Trans. A 35A (2004) 761–770.